DOI: 10.61782/fa.2025.0631

FORUM ACUSTICUM
EURONOISE 2025

NUMERICAL INVESTIGATION ON NOISE REDUCTION OF DISTRIBUTED PROPELLERS BY PHASE SYNCHRONIZATION

Zhe Yang[1*] **Matthias Meinke**[1] **Dominik Krug**[1] **Wolfgang Schröder**[1]
[1] Institute of Aerodynamics, RWTH Aachen University, Wüllnerstr. 5a, 52062 Aachen, Germany

ABSTRACT

Distributed propulsion systems represent a promising solution for future Urban Air Mobility (UAM) aircraft, offering benefits such as noise reduction, improved efficiency, and enhanced maneuverability. Recent studies highlight propeller phase synchronization as an effective active control strategy for mitigating noise in distributed propellers with compact installation clearance.

To further explore the mechanisms underlying noise reduction through phase synchronization, large-eddy simulations with adaptive mesh refinement are conducted to investigate co- and counter-rotating propeller pairs with relative phase angles of 0° and 90°. The far-field noise signals are predicted from the LES flow field by a time-domain formulation of the Ffowcs-Williams and Hawkings analogy. The results exhibit good agreement with wind tunnel measurements in terms of noise spectra and directivity patterns.

The findings indicate that synchronized propellers with a 90° relative phase angle achieve noise reductions greater than 20 dB at the blade passing frequency across all directions. Additionally, the acoustic signals of two isolated propellers are superimposed and compared with dual-propeller configurations. The observed tonal noise reduction is attributed to two key mechanisms: (a) reduced aerodynamic interaction at the propeller tips, which mitigates unsteady loading noise that propagates in the streamwise direction; and (b) destructive acoustic interference between counter-phase neighboring propellers.

*__Corresponding author__: z.yang@aia.rwth-aachen.de.
__Copyright__: ©2025 Zhe Yang et al. This is an open-access article distributed under the terms of the Creative Commons Attribution 3.0 Unported License, which permits unrestricted use, distribution, and reproduction in any medium, provided the original author and source are credited.

Keywords: distributed propulsion, propeller noise, phase synchronization, large eddy simulations.

1. INTRODUCTION

As a key driver of the emerging low-altitude economy, Urban Air Mobility (UAM) [1] has attracted significant attention as an innovative transportation solution. By leveraging advanced flight control and electric propulsion technologies, UAM aims to meet the increasing demand for efficient point-to-point travel in congested metropolitan areas or regions with limited road infrastructure. Despite its potential, the widespread adoption of UAM faces significant challenges, with aircraft generated noise being a major regulatory societal concern.

Among the various technologies explored for UAM applications, distributed electric propulsion (DEP) has emerged as a leading solution [2]. Characterized by multiple electrically driven propellers distributed along the airframe, DEP enhances aerodynamic performance, increases safety redundancy, provides acoustic shielding, and reduces propeller loading, thereby lowering overall noise emissions. Nonetheless, the compact installation of propellers introduces engineering challenges related to inter-propeller interactions and propeller–airframe coupling [3]. These complexities underscore the need for in-depth investigations into the noise and performance characteristics of DEP systems.

The aerodynamic and acoustic interactions between closely installed propellers have been the focus of extensive research. When the tip-to-tip separation is below 0.5 times the propeller diameter, significant thrust fluctuations have been observed [4–6], leading to a measurable reduction in propulsive efficiency, typically in the range of 1% to 2% [4, 7]. The interaction of tip vortices between adjacent propellers results in the distortion of he-

lical vortical structures [5, 8, 9], elevating turbulence intensity in the wake [4]. From an acoustic perspective, studies have reported increased noise levels at the blade passing frequency (BPF) and overall sound pressure level (OASPL) [4, 5]. Variations in sound pressure levels of up to ±10 dB at specific observation points have been documented [7], highlighting the significance of inter-propeller interactions in shaping the acoustic footprint of DEP systems. Additionally, noise source localization studies have identified the primary noise source within the gap region between adjacent propeller disks, where noise intensity is approximately 5 dB higher than that of blade tip noise [10]. This phenomenon is attributed to intensified blade-turbulence interactions and unsteady blade loading effects.

To mitigate noise emissions in DEP configurations, active noise control strategies, such as propeller phase synchronization, have been proposed. By precisely controlling the relative phase angles between adjacent propellers, this technique has demonstrated the potential to achieve noise reductions by 15 to 46 dB at the BPF and up to 6 dB in OASPL [11, 12]. The primary mechanism responsible for this noise reduction is destructive acoustic interference between phase-locked propellers [4]. However, recent findings indicate that reduced aerodynamic interactions between adjacent propellers also contribute significantly to noise mitigation [7, 9]. A comparative analysis of noise spectra from two-propeller configurations and superimposed isolated propeller signals further supports the coexistence of these two mechanisms [13]. Notably, in configurations with minimal tip clearance, nonlinear aerodynamic interactions become increasingly dominant, influencing overall noise emissions.

Building upon prior research, this study aims to further elaborate on the underlying mechanisms of noise reduction through propeller phase synchronization in distributed propulsion systems using high-fidelity numerical simulations. The paper is structured as follows: Section 2 provides an overview of the flow solver and numerical methodologies. Section 3 details the computational setup, including the test geometry and simulation parameters. Section 4 presents the results and discusses the key findings of the study. Finally, Section 5 summarizes the conclusions and outlines potential directions for future research.

2. NUMERICAL METHODS

Large-eddy simulations (LES) are performed based on the flow solver multiphysics-Aerodynamics Institute Aachen (m-AIA) [14]. The simulation workflow is illustrated in Fig. 1. First, an unstructured hierarchical Cartesian mesh is automatically generated by a parallel grid generator according to predefined mesh parameters for the target geometry. To track the rotating geometry of the propeller blades, a level-set solver based on the kinematic motion level-set approach [15] is employed, providing information about the surface location for solution adaptive mesh refinement (AMR) during the simulation run. The Navier-Stokes equations are solved by a finite-volume (FV) solver [16] at second-order accuracy in time and space to perform wall-resolved LES of the turbulent flow field. A postprocessing module is integrated into the simulation workflow to conduct time averaging or time-series data sampling on the dynamically changing mesh. For the far-field noise, Farassat's time-domain formulation 1A [17] of the Ffowcs-Williams and Hawkings (FW-H) method is used to predict the pressure signals at far-field observer positions. Dynamic load balancing (DLB) [18] is used to alleviate workload imbalances among the parallel processes generated by AMR to improve the computational efficiency on high-performance computing systems.

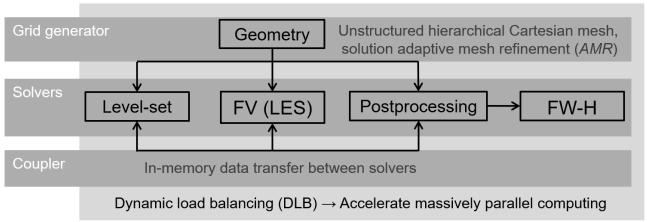

Figure 1. Overview of the m-AIA framework [14]

3. COMPUTATIONAL SETUP

3.1 Test geometry

Turhan et al. [12] have developed an experimental setup, shown in Fig. 2, to investigate the interaction noise of the closely arranged distributed propellers and evaluate the effectiveness of phase-synchronization for propeller noise reduction. The experiments were performed with two 2-bladed propellers manufactured by Mejzlik with a diameter of $D = 228.6\ mm$ (9 inch) and a pitch-to-

diameter ratio of $P/D = 1$. The center-to-center separation distance between adjacent propellers is $S/D = 1.05$. The two propellers were mounted 150 mm upstream of a supportive NACA0018 airfoil, with a chord length of $c_{wing} = 300$ mm, and a span of 940 mm.

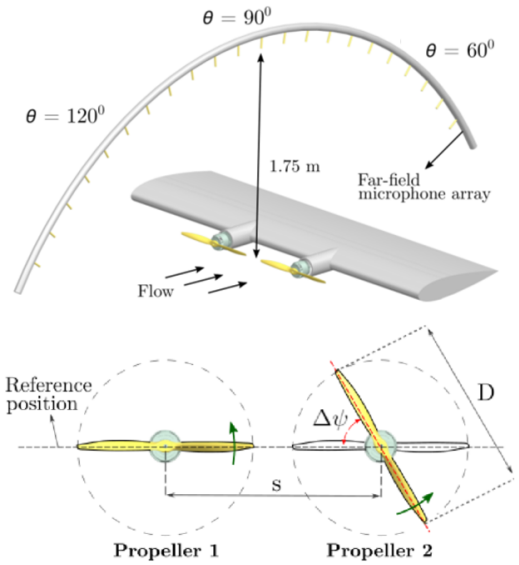

Figure 2. Experimental setup for propeller-propeller interaction noise [12].

The incoming freestream velocity is $U_\infty = 10$ m/s with a wing angle of attack $AoA = 0°$. The chord Reynolds number is approximately $Re_{wing} = 2 \cdot 10^5$. The two propellers rotate in the same direction at the speed of $n = 5000$ rpm, giving a blade tip tangential Mach number of about $M_{tip} = 0.17$, a blade passing frequency of $BPF = 166.7$ Hz and a propeller advance ratio of $J = U_\infty/(nD) = 0.53$. Two propeller blade relative phase angles, $\Delta\psi = 0°$ and $90°$ are tested.

3.2 Flow simulation setups

Based on the previous experimental/numerical observations by [19, 20] that the propeller-propeller interaction is a major noise source of the distributed propulsion system and has a much higher contribution to the far-field noise than the propeller-airfoil interaction, the flow field of only the two propellers are simulated and the supportive nacelle and airfoil are omitted to reduce the computational cost. The lengths $L_x = 1400$ mm, $L_y = 1200$ mm, and $L_z = 1000$ mm define the size of the computational domain. The no-slip boundary condition is imposed on all surfaces which are assumed to be adiabatic. Subsonic inlet and outlet conditions with an acoustic sponge layer are used for the far-field boundaries to absorb any spurious reflected pressure waves.

The computational mesh is shown in Fig. 3. To resolve the turbulent boundary layer near the solid surfaces, the minimum spatial step near solid surfaces is $4.3 \cdot 10^{-5}$ m. Approximately 300 cells are distributed along the propeller chord. Adaptive mesh refinement is applied to the fluid-solid interface with the minimum spatial resolution and coarsening towards the far field until a maximum spatial step of $1.4 \cdot 10^{-3}$ m is reached. Patch refinement boxes are implemented in the near field to better resolve the propeller slipstream. Overall, this leads to approximately $500 \cdot 10^6$ cells. The rotating propeller and the high-frequency turbulent scales are resolved by a time step of $1 \cdot 10^{-7}$ s, which is determined by the stability limit of the numerical method.

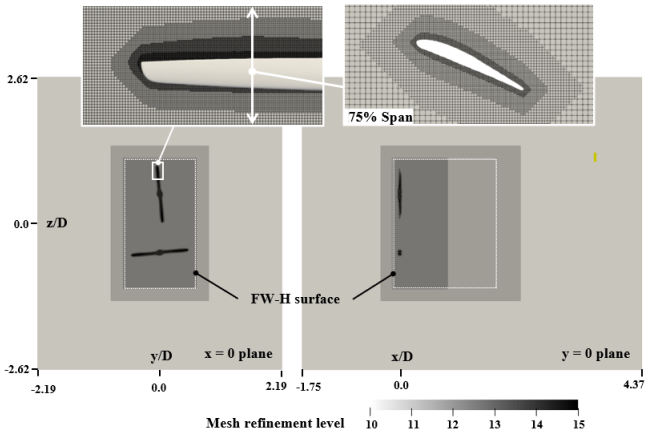

Figure 3. Illustration of the computational domain and mesh

3.3 Far-field noise prediction setups

A permeable FW-H surface around the vortex core of the propeller pairs is employed to record the near-field perturbations. The surface is a rectangular box, as defined by the white dashed lines in Fig. 3. The leeward side of the FW-H surface is left open to avoid spurious noise generated by hydrodynamic perturbations traveling over the sampling surface. The spatial resolution of the sampling surface is $2 \cdot 10^{-3}$ m. The sampling frequency is 65 kHz and data for 10 propeller revolutions are recorded.

4. RESULTS

4.1 Flow field

The generation and propagation of the instantaneous vortex structures of the co-rotating propeller pairs with relative phase angle $\Delta\psi = 0°$ are shown in Fig. 4.

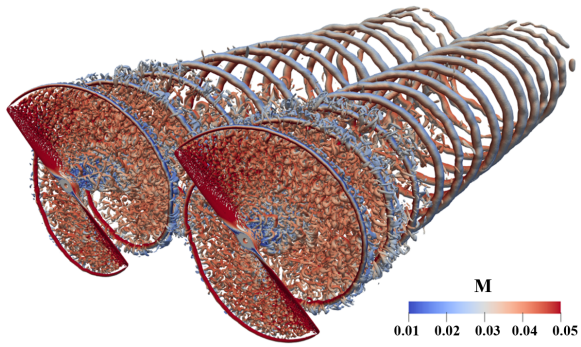

Figure 4. Vortex structures denoted by the Q-criterion [21] with an iso-surface value of $\tilde{Q} = 2$.

The time-averaged statistics of the thrust coefficient $C_T = F_T/(\rho_0 n^2 D^4)$ is provided in Tab. 1. The time histories of the thrust coefficient for propeller 1 at relative phase angles of $\Delta\psi = 0°$ and $90°$ are illustrated in Fig. 5, co-rotating propellers in Fig. 5 (a) and counter-rotating propellers in Fig. 5 (b). Both cases are compared against the isolated propeller.

The results indicate that closely installed propeller pairs exhibit an approximately 0.5% higher time-averaged thrust coefficient compared to an isolated propeller. Furthermore, the time-averaged thrust coefficient at a relative phase angle of $\Delta\psi = 0°$ is slightly higher than that at $\Delta\psi = 90°$.

The instantaneous thrust coefficients of installed propeller pairs show clear periodic fluctuations dominated by the blade passing frequency (BPF). The root-mean-square fluctuation of the thrust coefficient at a relative phase angle of $\Delta\psi = 0°$ is roughly 45% higher than that of an isolated propeller. For the $\Delta\psi = 90°$ phase angle, this increase reduces to about 24%. This demonstrates that adopting a relative phase angle of $\Delta\psi = 90°$ helps mitigate aerodynamic interference between adjacent propellers, and reduce periodic unsteady loading on the blades.

To further investigate the aerodynamic interactions between adjacent propellers, Fig. 6 presents the total pressure perturbation at the propeller tip gap located at

Table 1. Time-averaged thrust coefficient of propeller 1.

	C_T	C_{Trms}
Isolated propeller	0.083 25	0.000 62
co-r, $\Delta\psi = 0°$	0.083 68	0.000 92
co-r, $\Delta\psi = 90°$	0.083 63	0.000 78
counter-r, $\Delta\psi = 0°$	0.083 74	0.000 89
counter-r, $\Delta\psi = 90°$	0.083 62	0.000 76

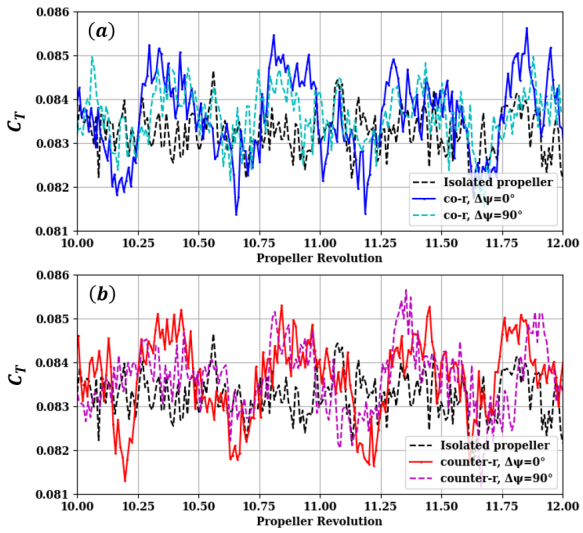

Figure 5. Time history of the propeller thrust coefficient of propeller 1; (a) co-rotating propellers, (b) counter-rotating propellers.

$(x, y, z) = (0, 0, 0)$. The nondimensional perturbed total pressure is defined as $\tilde{p_T'} = (p_T - \bar{p}_T)/(0.5\rho_\infty U_\infty^2)$. For an isolated propeller, the total pressure fluctuation at the blade tip exhibits periodicity corresponding to the blade passing frequency, with a clear pressure drop when each blade passes.

Considering the installed propeller pairs with a relative phase angle of $\Delta\psi = 0°$, the amplitude of the total pressure fluctuation approximately doubles due to simultaneous blade passages from both propellers through the tip gap. However, at a phase angle of $\Delta\psi = 90°$, the total pressure fluctuations are periodic at twice the rotor frequency, as blades from each propeller pass through the tip gap alternately. The fluctuation amplitude in this scenario is comparable to that of an isolated propeller. Moreover,

the rotation direction of the propellers has negligible influence on the total pressure fluctuations at the blade tip.

A comparison between Fig. 5 and Fig. 6 reveals that variations in total pressure fluctuations in the tip gap align closely with changes in propeller thrust. This correlation suggests that aerodynamic interference between adjacent propellers significantly contributes to unsteady aerodynamic loading on the rotor, which potentially increase noise generation.

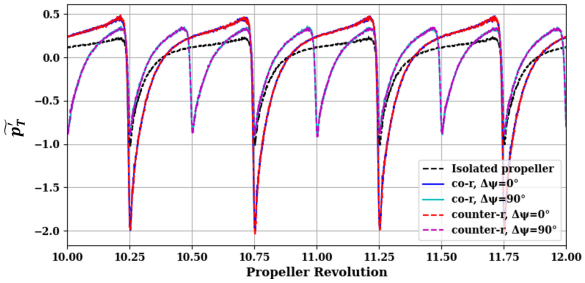

Figure 6. Total pressure perturbation in the tip gap.

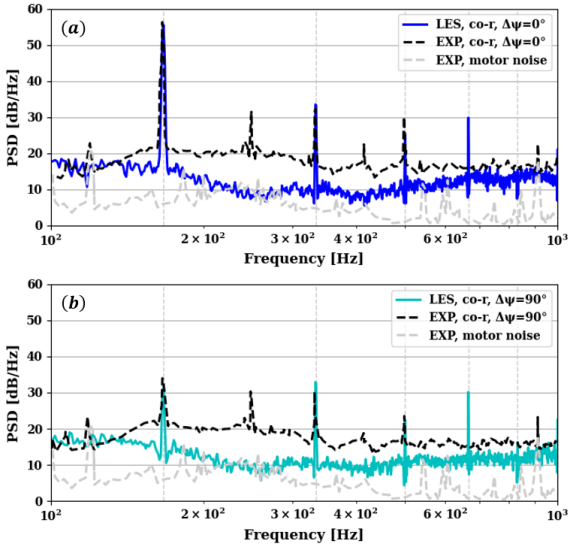

Figure 7. Predicted power spectral density of the co-rotating propeller pairs with relative phase angle (a) $\Delta\psi = 0°$, and (b) $\Delta\psi = 90°$.

4.2 Acoustic Field

The far-field noise of the synchronized propellers is determined by the permeable FW-H approach and compared with the wind tunnel measurements from [12]. The microphone is located 1.75 m off the propeller in the vertical plane with an angular position of $\theta = 90°$. The power spectral density (PSD) of the acoustic signal is calculated using Welch's method, 50% overlap, filtered by a Hanning window, with a frequency resolution of $\Delta f = 1.0\ Hz$, and the reference pressure is $2 \cdot 10^{-5}\ Pa$. The grey dashed lines in the plots represent the propeller blade passing frequency (BPF) and its harmonics.

Fig. 7 compares the predicted far-field noise spectra with the experimental reference data in the frequency range from 100 Hz to 1000 Hz. It can be seen that the propeller tonal noise at the first and second BPF frequencies is accurately predicted by the numerical method. The reference data showed a higher amplitude of broadband noise, which was mainly caused by the background motor noise in the wind tunnel experiment.

Next, the predicted noise spectra at the angular position of $\theta = 90°$ for cases with different rotation directions and relative phase angles are shown in Fig. 8. No significant difference in broadband noise was observed among the cases; variations mainly occurred in propeller tonal noise. A close look at the first two blade passing frequencies (BPF) reveals that the relative phase angle primarily affects the first BPF. At a relative phase angle of $\Delta\psi = 0°$, cases with different rotation directions exhibited similar far-field noise levels of approximately 55 dB at the first BPF. In contrast, at $\Delta\psi = 90°$, the first BPF noise level for the co-rotating case decreased by about 24 dB. Remarkably, in the counter-rotating case at $\Delta\psi = 90°$, the first BPF tonal noise was nearly eliminated, achieving a noise reduction exceeding 50 dB. This finding is consistent with experimental results reported by Shao et al. [11]. As a trade-off for the reduction in the first BPF, the second BPF tonal noise increases by approximately 1 dB for the cases with a $\Delta\psi = 90°$ relative phase angle. The above findings evidence that propeller phase synchronization effectively reduces the first BPF tonal noise, especially for counter-rotating propellers.

The directivity of the propeller far-field noise compared with experimental measurements is presented in Fig. 9. Fig. 9 (a) shows the sound pressure level (SPL) at the first BPF and Fig. 9 (b) illustrates the overall sound pressure level (OASPL) within the frequency range of 100 to 1000 Hz. As shown in Fig. 9 (a), the numerical predictions agree well with the experimental data upstream of the propeller but underestimate the SPL downstream. This

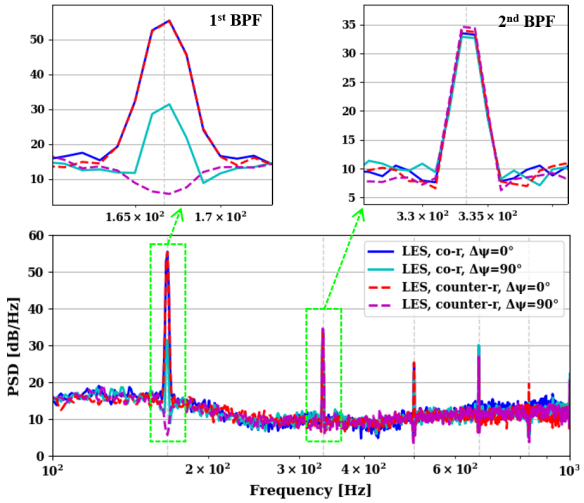

Figure 8. Comparison of predicted noise spectra for several test cases.

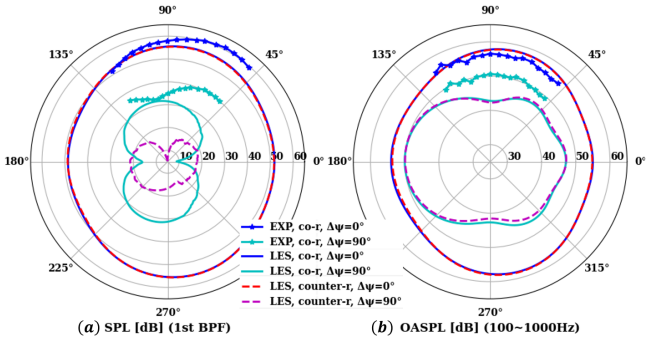

Figure 9. Directivity of the propeller noise.

discrepancy may arise from the scattering effect of the airfoil located downstream in the experiment, which alters the directivity of the sound field. A similar discrepancy was observed by Turhan et al. [22] in their mid-fidelity Vortex Lattice Method (VLM) simulations with the same test geometry. Consistent with Fig. 8, noise directivities for cases with a relative phase angle of $\Delta\psi = 0°$ are nearly identical. A relative phase angle of $\Delta\psi = 90°$ reduces far-field noise by over 20 dB at the first BPF in all directions. Compared to co-rotating propellers, counter-rotating propellers achieve an additional 10 dB noise reduction at $\theta = 90°$ and 270°, i.e. perpendicular above and below the propeller.

For the OASPL shown in Fig. 9 (b), numerical predictions at $\Delta\psi = 0°$ match very well with the experimental data, whereas at $\Delta\psi = 90°$, the numerical results exceed the experimental values on the top and bottom sides. The reduction of the OASPL ranges from 5 to 15 dB for different directions. The findings reveal that a staggered relative phase angle $\Delta\psi = 90°$ significantly reduces the overall noise levels in all directions, while the influence of different rotation directions on the OASPL is negligible.

4.3 Superposition of the isolated propeller noise

The principle of superposition [13] is employed to further understand noise-reduction mechanisms due to propeller phase synchronization. The far-field noise signal of a simulated isolated propeller is spatially and temporally shifted to construct a two-propeller system identical to the experimental setup but without aerodynamic interactions. The noise signals from these two isolated propellers are linearly superimposed to represent the dual-propeller noise, accounting only for acoustic interference. A comparison of the superimposed results with direct dual-propeller simulations in Fig. 10 shows the contributions from aerodynamic interactions and purely acoustic interference between adjacent propellers to far-field noise can be distinguished.

Figs. 10 (a) and (c) show the far-field noise for co-rotating and counter-rotating propeller pairs at a relative phase angle $\Delta\psi = 0°$. The isolated superimposed propellers exhibit a dipole-like directivity for the first BPF noise, with acoustic energy mainly concentrated on the top and bottom sides of the propellers, and relatively low noise levels upstream and downstream. In contrast, the dual-propeller simulation results show significantly increased noise upstream and downstream of the propellers. Specifically, tonal noise levels at $\theta = 0°$ and 180° increase by approximately 30 dB. This indicates that aerodynamic interactions between adjacent propellers generate strong additional noise sources, primarily propagating upstream and downstream.

Fig. 10 (b) presents the far-field noise of co-rotating propeller pairs at a relative phase angle of $\Delta\psi = 90°$. Due to the reduced aerodynamic interactions at the blade tips, the dual-propeller simulation results exhibit dipole patterns consistent with those predicted by linear superposition. Destructive wave interactions occur at the far-field microphone locations due to the phase difference between the two propellers, leading to a significant reduction in noise levels. The pure acoustic noise cancellation is most pronounced in the case of counter-rotating propellers with

$\Delta\psi = 90°$. As shown in Fig. 10 (d), the first BPF noise is nearly completely eliminated, such that the noise level is reduced to that of the background broadband noise.

In addition, we observed that in certain cases, such as at $\theta = 0°$ in Figs. 10 (a), (b), and (c), the noise level of the dual-propeller simulations are lower than the predicted value based on linear superposition. This indicates the presence of nonlinear effects in the dual-propeller case, which influence the directivity of propeller far-field noise.

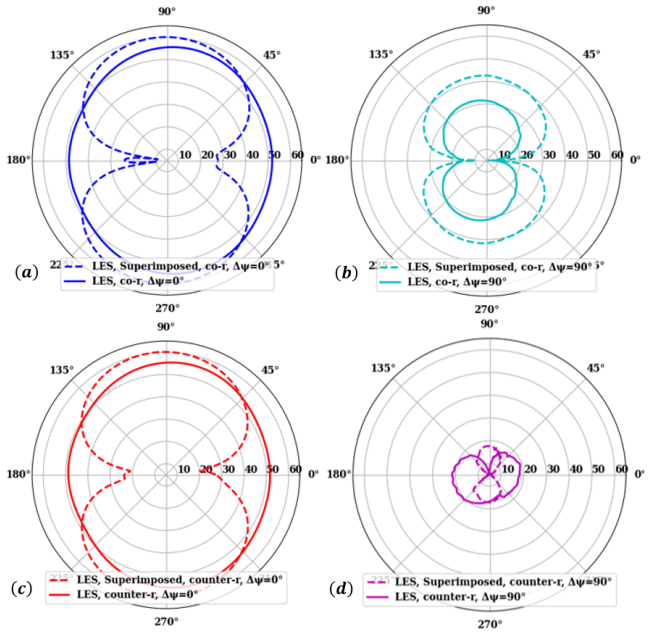

Figure 10. Comparison of first BPF noise directivity of the superimposed propellers and simulated propeller pairs.

5. CONCLUSIONS

The noise reduction mechanisms of distributed propeller systems through phase synchronization are investigated by a hybrid LES/FW-H approach. The numerical method accurately captures aerodynamic interactions and acoustic interference between adjacent propellers and is validated against wind tunnel measurements.

Results show that the relative phase angle of $\Delta\psi = 90°$ effectively reduces the tonal noise at the first blade passing frequency. Specifically, the co-rotating configuration achieves a noise reduction of approximately 24 dB, while the counter-rotating configuration yields an even greater reduction, with the first BPF tonal noise reduced by over 50 dB. Additionally, phase synchronization leads to an overall sound pressure level reduction of 5 to 15 dB, depending on the direction.

The observed noise reduction is primarily attributed to two mechanisms: (1) a reduction in aerodynamic interactions at the propeller tips, which mainly propagate upstream and downstream, and (2) destructive acoustic interference between counter-phase neighboring propellers which effectively cancels the first BPF noise component, particularly in counter-rotating configurations.

The present work offers practical insights into integrating phase synchronization in urban air mobility propulsion systems, emphasizing dual control of aerodynamic and acoustic sources. Future research could investigate additional propeller parameters, including tip clearance variations, transitional inflow conditions, elastic propeller blades, and multi-propeller configurations, to further refine noise mitigation strategies.

6. ACKNOWLEDGMENTS

The present work has received funding from the European Union's Horizon 2020 research and innovation program under the project ENODISE (Enabling optimized disruptive airframe-propulsion integration concepts) (`www.vki.ac.be/index.php/about-enodise`) grant agreement No. 860103. The authors would like to thank B. Turhan and M. Azarpeyvand from the University of Bristol (United Kingdom) for providing the test geometry and experimental data. The authors also gratefully acknowledge the Gauss Centre for Supercomputing e.V. (`www.gauss-centre.eu`) for funding this project by providing computing time on the GCS Supercomputer HAWK at Höchstleistungs-Rechenzentrum Stuttgart (`www.hlrs.de`).

7. REFERENCES

[1] A. Straubinger, R. Rothfeld, M. Shamiyeh, K.-D. Büchter, J. Kaiser, and K. O. Plötner, "An overview of current research and developments in urban air mobility–setting the scene for uam introduction," *Journal of Air Transport Management*, vol. 87, p. 101852, 2020.

[2] A. S. Gohardani, G. Doulgeris, and R. Singh, "Challenges of future aircraft propulsion: A review of distributed propulsion technology and its potential application for the all electric commercial aircraft,"

Progress in Aerospace Sciences, vol. 47, no. 5, pp. 369–391, 2011.

[3] E. Greenwood, K. S. Brentner, R. F. Rau, and Z. F. Ted Gan, "Challenges and opportunities for low noise electric aircraft," *International Journal of Aeroacoustics*, vol. 21, no. 5-7, pp. 315–381, 2022.

[4] W. Zhou, Z. Ning, H. Li, and H. Hu, "An experimental investigation on rotor-to-rotor interactions of small uav propellers," in *35th AIAA Applied Aerodynamics Conference*, p. 3744, 2017.

[5] H. Lee and D.-J. Lee, "Rotor interactional effects on aerodynamic and noise characteristics of a small multirotor unmanned aerial vehicle," *Physics of Fluids*, vol. 32, no. 4, 2020.

[6] A. D. Thai, E. De Paola, A. Di Marco, L. G. Stoica, R. Camussi, R. Tron, and S. M. Grace, "Experimental and computational aeroacoustic investigation of small rotor interactions in hover," *Applied Sciences*, vol. 11, no. 21, p. 10016, 2021.

[7] R. de Vries, N. van Arnhem, T. Sinnige, R. Vos, and L. L. Veldhuis, "Aerodynamic interaction between propellers of a distributed-propulsion system in forward flight," *Aerospace Science and Technology*, vol. 118, p. 107009, 2021.

[8] D. Shukla and N. Komerath, "Multirotor drone aerodynamic interaction investigation," *Drones*, vol. 2, no. 4, p. 43, 2018.

[9] A. Zarri, A. Koutsoukos, and F. Avallone, "Aerodynamic and acoustic interaction effects of adjacent propellers in forward flight," in *AIAA Aviation 2023 Forum*, p. 4489, 2023.

[10] T. Zhou, H. Jiang, and X. Sun, "Noise source imaging measurements for small-scale multi-propeller systems," *Applied Acoustics*, vol. 194, p. 108801, 2022.

[11] M. Shao, Y. Lu, X. Xu, S. Guan, and J. Lu, "Experimental study on noise reduction of multi-rotor by phase synchronization," *Journal of Sound and Vibration*, vol. 539, p. 117199, 2022.

[12] B. Turhan, H. K. Jawahar, A. Gautam, S. Syed, G. Vakil, D. Rezgui, and M. Azarpeyvand, "Acoustic characteristics of phase-synchronized adjacent propellers," *The Journal of the Acoustical Society of America*, vol. 155, no. 5, pp. 3242–3253, 2024.

[13] M. Bhardwaj, T. P. Chong, C. Paruchuri, and P. Joseph, "Noise decomposition of dual synchronized propellers in hover," in *30th AIAA/CEAS Aeroacoustics Conference (2024)*, p. 3045, 2024.

[14] Institute of Aerodynamics, RWTH Aachen University, "m-AIA multiphysics flow solver." `https://doi.org/10.5281/zenodo.13350586`, 2024.

[15] A. Pogorelov, L. Schneiders, M. Meinke, and W. Schröder, "An adaptive cartesian mesh based method to simulate turbulent flows of multiple rotating surfaces," *Flow, Turbulence and Combustion*, vol. 100, pp. 19–38, 2018.

[16] M. Meinke, W. Schröder, E. Krause, and T. Rister, "A comparison of second-and sixth-order methods for large-eddy simulations," *Computers & Fluids*, vol. 31, no. 4-7, pp. 695–718, 2002.

[17] K. S. Brentner and F. Farassat, "Analytical comparison of the acoustic analogy and kirchhoff formulation for moving surfaces," *AIAA Journal*, vol. 36, no. 8, pp. 1379–1386, 1998.

[18] A. Niemöller, M. Schlottke-Lakemper, M. Meinke, and W. Schröder, "Dynamic load balancing for direct-coupled multiphysics simulations," *Computers & Fluids*, vol. 199, p. 104437, 2020.

[19] T. Sinnige, B. D. Corte, R. De Vries, F. Avallone, R. Merino-Martínez, D. Ragni, G. Eitelberg, and L. L. Veldhuis, "Alleviation of propeller-slipstream-induced unsteady pylon loading by a flow-permeable leading edge," *Journal of Aircraft*, vol. 56, no. 3, pp. 1214–1230, 2019.

[20] Y. Zhe, M. Meinke, and W. Schröder, "Numerical analysis of propeller-airfoil interaction in a distributed propulsion system using a hybrid LES and FW-H approach," in *30th AIAA/CEAS Aeroacoustics Conference (2024)*, p. 3211, 2024.

[21] J. Jeong and F. Hussain, "On the identification of a vortex," *Journal of Fluid Mechanics*, vol. 285, pp. 69–94, 1995.

[22] B. B. Turhan, L. F. Lopes de Moraes Filho, S. Pullin, B. Y. Zhou, H. K. Jawahar, A. Gautam, D. Rezgui, and M. Azarpeyvand, "Numerical and experimental analysis of synchronized propellers for noise mitigation," in *30th AIAA/CEAS Aeroacoustics Conference (2024)*, p. 3237, 2024.